PEER-REVIEWED · OPEN ACCESS
Sriwijaya Journal of Forensic and Medicolegal
Vol. 4, No. 1 (2026), pp. 15–25 · e-ISSN 2987-1530 · Article ID: 334
journal homepage: phlox.or.id/index.php/sjfm

Original Research Article

Human Blood Thanatotranscriptome Dynamics and Cross-Donor Generalisability of Postmortem Interval Prediction: A Longitudinal RNA-seq Reanalysis

Rachmat Hidayat[1*], Khairiel Anwar[2]

[1]*Department of Medical Biology, Faculty of Medicine, Universitas Sriwijaya, Palembang, Indonesia*
[2]*Department of Biomolecular Science, CMHC Research Center, Palembang, Indonesia*

ARTICLE INFO

Article history
Received: April 10, 2026
Revised: April 29, 2026
Accepted: May 25, 2026
Available online: May 27, 2026
Published: May 30, 2026

Keywords
Blood
Cross-donor validation
Postmortem interval
RNA sequencing
Thanatotranscriptome

Corresponding author
Rachmat Hidayat
E-mail: dr.rachmat.hidayat@gmail.com
ORCID: 0000-0001-5770-1201

DOI
https://doi.org/10.59345/sjfm.v4i1.334

ABSTRACT

Background. Thanatotranscriptomic profiles may encode time-dependent molecular changes after death, but forensic utility requires temporal signals that generalise across individuals.

Objective. To characterise the genes and molecular pathways that change consistently with absolute postmortem interval (PMI) in serial human postmortem blood samples.

Methods. We reanalysed processed counts from 54 serial postmortem blood samples of seven individuals in GSE163207, spanning an absolute PMI of 2.35-37.83 h. After expression filtering and trimmed mean of M-values normalisation, limma-voom models included individual fixed effects and continuous absolute PMI. Eligible genes required a Benjamini-Hochberg false-discovery rate <0.05, an absolute log2 change >=0.10 per 10 h, and concordant direction in at least five individuals. Enrichment used the expressed-gene background. Nested leave-one-individual-out elastic-net validation kept feature selection and tuning within training donors.

Results. Among 12,633 expressed genes, 1,976 were eligible (954 increasing; 1,022 decreasing). Increasing genes were enriched for cytoskeletal, extracellular-matrix, oxidative-stress, and mitochondrial processes; decreasing genes were enriched for adaptive immune and antigen-presentation pathways. Sensitivity analysis produced an effect correlation of 0.987, with 1,645 genes retaining significance and direction. Cross-donor prediction yielded an RMSE of 10.03 h (95% CI 8.12-11.32), MAE of 8.63 h (95% CI 6.33-10.40), and R2 of -0.219, underperforming the training-mean baseline.

Conclusion. Human blood undergoes reproducible early postmortem molecular remodelling, but this seven-individual cohort does not support generalisable individual PMI prediction.

How to cite. Hidayat R, Anwar K. Human blood thanatotranscriptome dynamics and cross-donor generalisability of postmortem interval prediction: a longitudinal RNA-seq reanalysis. Sriwijaya J Forensic Medicoleg. 2026;4(1):15–25.

1. Introduction

Estimating the postmortem interval (PMI) is a fundamental task in forensic medicine because elapsed time can influence scene reconstruction, interpretation of injuries, evaluation of witness accounts, and selection of laboratory examinations. Classical approaches integrate algor mortis, rigor mortis, livor mortis, supravital reactions, decomposition, entomology, and contextual information, but environmental and individual variation usually make a reasoned interval more defensible than an exact time point. Recent syntheses therefore position molecular measurements as complementary evidence rather than replacements for the integrated forensic assessment.[1,2]

RNA-based approaches are attractive because the transcriptome is dynamic and biologically structured. After circulatory arrest, oxygen and nutrient delivery cease, energy-dependent processes become progressively disrupted, membrane integrity changes, and stress-response pathways may be activated or extinguished at different rates. The human blood dataset analysed here demonstrated coordinated cell-survival and DNA-damage-repair signals shortly after death, while recent transcriptomic experiments in other tissues have identified time-associated expression changes in postmortem material.[3-7]

Together, these studies argue against a model of uniform transcript loss and support tissue-specific mixtures of regulation, selective stability, cell survival, and compositional change.

The same biological responsiveness that makes RNA informative also makes it sensitive to the measurement context. Temperature and delay before preservation can alter degradation patterns; RNA quality metrics vary across postmortem specimens; and increasing PMI can attenuate disease-associated expression signatures.[8-10] Blood adds further heterogeneity through leukocyte composition, premortem inflammation, age, disease, medication, terminal events, source vein, sequencing depth, and technical batch. A temporal signal may therefore be detectable after adjustment for a donor's baseline while remaining difficult to distinguish from the molecular identity of a new individual.

Recent primary studies have broadened the candidate marker space beyond conventional messenger RNA. MicroRNA transcriptome profiling, long non-coding RNA degradation, temperature-aware circular RNA models, targeted circRNA combinations, molecular-beacon detection of miR-133a-5p, and combined endogenous and exogenous small-RNA signatures have each demonstrated time-dependent molecular information in specific tissues or experimental systems.[11-16]

These findings expand biological discovery, but their practical value depends on assay stability, prespecified prediction targets, donor-level separation, and independent human validation.

Tissue and assay selection also determine how a marker could be translated. Recent work has evaluated mRNA in human dental pulp and skeletal muscle, postmortem gene expression in murine liver, and reverse-transcription yield in forensic samples using droplet digital PCR.[17-20] Such studies support a staged pathway from sequencing-based discovery to a parsimonious panel measured with analytically characterised assays. They also show why the intended matrix, postmortem window, normalisation strategy, and measurement platform must be defined before prediction performance can be interpreted.

Complementary molecular layers provide a wider perspective on transportability. Metabolomic and volabolomic studies have modelled PMI across human and animal materials, different organs, causes of death, and ambient temperatures, while proteomic work has examined long-term changes in human bone.[21-,26] Microbiome studies have likewise demonstrated time-associated succession in oral communities, cold-environment decomposition, submerged skeletal remains, soil, and insect-influenced cadavers.[27,-31] Their collective lesson is not that one modality is universally superior, but that apparent temporal structure must be evaluated under validation splits that match the intended case-level use.

Antiga et al. generated GSE163207, a rare longitudinal human blood RNA-sequencing resource consisting of 54 postmortem samples from seven individuals.[3] The serial design permits estimation of temporal movement within individuals but creates dependence among samples from the same donor. It also contains a 0-24 h sampling offset from each donor's first collection and an absolute PMI from death to collection; the first sample was not obtained at death, so the forensic outcome spans 2.35-37.83 h. The novelty of this study is the integrated evaluation of longitudinal biological signal and cross-donor predictive transportability within this same dataset, using absolute PMI, donor-adjusted gene association, direction-consistency criteria, expressed-background pathway analysis, sensitivity analysis, and strictly nested leave-one-individual-out validation. The primary aim was to characterise genes and molecular pathways that change consistently with absolute PMI in serial human postmortem blood samples. The secondary aim was to determine whether those signals could predict absolute PMI in a completely unseen donor and outperform a training-mean baseline. We hypothesised that structured within-donor expression changes would be detectable, whereas cross-donor prediction would remain sensitive to inter-individual heterogeneity in this seven-donor cohort.

2. Methods

2.1 Study design and data source

This study was a secondary longitudinal analysis of the publicly available GSE163207 dataset in the NCBI Gene Expression Omnibus.[3] The source dataset contains processed RNA-seq gene counts and sample metadata for 54 postmortem blood samples collected serially from seven deceased individuals. Five individuals were male and two were female, ages ranged from 56 to 89 years, and sequencing was performed using an Illumina NextSeq 500 platform. Individual donors contributed between three and nine samples. All available samples with an identifiable donor and absolute PMI were included. Because the cohort was fixed by the public resource, no prospective sample-size calculation or participant recruitment was undertaken for the present analysis.

Two analytical questions were defined before modelling. The association question concerned the average change in transcript abundance per ten hours of absolute PMI after accounting for stable differences between individuals. Its observational unit was the serial blood sample, with donor fixed effects used to isolate within-donor temporal information. The prediction question concerned the error expected when estimating absolute PMI for an individual absent from all stages of model development. For this question, the independent generalisation unit was the donor. Thus, the 54 samples increased temporal resolution but did not replace the seven individuals as the effective units for evaluating transportability to a new case.

The primary time variable was absolute PMI in hours, calculated in the source metadata from death to each blood collection. Absolute PMI ranged from 2.35 to 37.83 h. Serial offsets ranged from 0 to 24 h and represented time since the first sample from the same donor. These offsets were used to describe sampling schedules but were not substituted for absolute PMI in association or prediction models. The main biological outcome was the continuous gene-expression response to absolute PMI. The predictive outcome was continuous absolute PMI in hours. No diagnostic threshold, categorical PMI window, or claim of forensic decision accuracy was prespecified.

2.2 Ethics

The source investigation reported approval by the Ethical Commission of the University Hospitals Leuven (S58486) and informed consent obtained before donation.[3] The present work used de-identified data made publicly available through GEO and involved no contact with donors or relatives. Ethical approval for the secondary analysis was granted by the CMHC Ethics Committee Indonesia (No. 009/CMHC/Ethics/08/2026). The analysis was limited to the scientific objectives described in this manuscript, and no attempt was made to re-identify individuals from genomic or clinical information.

2.3 Data processing and quality assessment

The GEO series matrix and processed count archive were downloaded from the GSE163207 record. Sample

accessions were linked to individual identifier, age, sex, source vein, sampling offset, and absolute PMI. Metadata labels were standardised without changing their substantive meaning. Each GEO accession occurred once, every sample had a recorded absolute PMI, and all 54 count files could be reconciled with the series matrix. Gene rows were indexed by Ensembl identifiers and checked for duplicated records before concatenation. The resulting raw count matrix contained 60,204 gene rows across 54 samples.

Library size, number of detected genes, missing values, duplicate identifiers, and consistency of the serial schedule were examined before inferential analysis. Library totals ranged from 3.84 to 27.03 million counts, with a median of 13.51 million. The number of genes with non-zero counts per sample ranged from 12,422 to 17,803, with a median of 15,711. Six libraries had total counts below 50% of the cohort median. They were retained in the primary analysis to preserve each donor's observed longitudinal series, and their influence was examined in a sensitivity model. The library-size flag was used as an analytical criterion and was not interpreted as a complete assessment of RNA integrity, because read-level quality measurements and RNA integrity numbers were not available in the processed-count files.

Expression filtering was performed before normalisation. Genes were retained when counts per million were at least one in seven or more samples, corresponding to approximately 13% of the 54-sample cohort. This rule removed transcripts with insufficient information for stable estimation while allowing signals expressed in a subset of donors or time points. A total of 12,633 genes passed the filter and defined the expressed-gene universe for subsequent modelling and enrichment. Counts were stored in an edgeR DGEList and normalised with the trimmed mean of M-values method to account for compositional differences among libraries.

Normalised counts were transformed with the voom procedure, which estimates the mean-variance relation and assigns observation-level precision weights for linear modelling. Principal-component analysis was performed on the 500 genes with the greatest variance in voom expression. The analysis was descriptive: it was used to visualise donor structure, temporal movement, and potential sample separation, not to select samples or test a formal hypothesis. Aggregate increasing and decreasing signatures were calculated after donor centring so that their plotted trajectories reflected temporal movement relative to each donor's average rather than unadjusted differences in baseline expression.

2.4 Longitudinal association and sensitivity analysis

For each of the 12,633 expressed genes, a limma-voom linear model included categorical individual fixed effects and continuous absolute PMI. The model can be written as $y_{gij} = \alpha_{gi} + \beta_g \times PMI_{ij} + \varepsilon_{gij}$, where y_{gij} is the weighted $\log_2$ expression of gene g for individual i at observation j, α_{gi} is the gene-specific fixed effect for that individual, β_g is the common absolute-PMI slope, and ε_{gij} is the residual term. Individual fixed effects absorbed time-invariant baseline differences among the seven donors, whereas the PMI coefficient estimated the mean within-donor temporal slope. The coefficient was multiplied by ten and reported as $\log_2$ expression change per ten hours of absolute PMI. A positive value indicated increasing expression with time and a negative value indicated decreasing expression. The model did not include a donor-by-time interaction because the primary estimand was the common temporal direction, and the number and schedule of samples differed among donors.

Raw P values for the PMI coefficient were adjusted across genes by the Benjamini-Hochberg false-discovery-rate procedure. A transcript was considered eligible for biological interpretation only when three conditions were met: adjusted $P < 0.05$, absolute $\log_2$ change of at least 0.10 per ten hours, and a slope direction concordant with the overall coefficient in at least five of seven donor-specific simple regressions. The effect-size criterion excluded statistically detectable but very small changes, while the direction rule reduced dependence on a pattern concentrated in a minority of donors. These thresholds were applied jointly and before selection of representative genes for tables or pathway analysis.

The direction-consistency calculation was supplementary to the fixed-effect model. Within each donor, voom expression for a gene was regressed on absolute PMI when the donor had sufficient serial observations, and the sign of that slope was compared with the sign of the primary coefficient. The number of concordant donors was recorded for every transcript. This procedure did not generate a separate significance test for each donor and did not require individual slopes to be statistically significant. Its purpose was to document whether the direction of change was broadly shared across the available longitudinal series.

Sensitivity analysis examined the combined influence of library size and blood-collection site. The six libraries below 50% of the median library total were excluded, and a femoral-versus-subclavian vein indicator was added to the donor-adjusted absolute-PMI model. Robustness was assessed by the Pearson correlation between primary and sensitivity PMI coefficients across expressed genes and by counting eligible genes that retained the same direction and adjusted $P < 0.05$. Because exclusion reduced the number of observations and the vein distribution was not balanced independently of donor, the sensitivity model was interpreted as a stability analysis rather than a replacement primary analysis.

2.5 Functional enrichment

Eligible increasing and decreasing genes were analysed separately to preserve the biological distinction between pathways whose member transcripts accumulated and pathways whose member transcripts declined with absolute PMI. Within each direction, genes were ranked by adjusted P value and the 500 highest-ranked eligible genes were submitted to g:Profiler g:GOSt. Enrichment was queried for Gene Ontology Biological Process, Reactome, and Kyoto Encyclopedia of Genes and Genomes terms. The full set of 12,633 expressed genes was supplied as a custom statistical background, preventing unexpressed genes from defining the reference universe. The application programming interface mapped 495 increasing and 497 decreasing query identifiers.

Multiplicity was controlled using false-discovery-rate correction within the enrichment procedure. Ontology resources contain nested and overlapping terms; therefore, results were reviewed by direction and biological theme, and representative terms were selected for the main figure to reduce semantic repetition. Selection for presentation considered adjusted significance, number of overlapping genes, term specificity, and relevance to the postmortem blood setting. Complete machine-readable enrichment results were retained in the analysis archive. Enrichment was treated as a description of coordinated

transcript membership, not as evidence of causal regulation, protein abundance, enzymatic activity, or metabolic flux.

2.6 Cross-donor prediction

Predictive performance was evaluated with strict nested leave-one-individual-out validation. In each of seven outer folds, all serial samples from one donor were withheld as the test set and the remaining donors formed the development set. No expression measurement, PMI value, feature ranking, or tuning result from the held-out donor was available during model development. This separation was maintained because serial samples from one person share a molecular background and should not be regarded as independent test observations when the intended application is prediction in a new individual.

Feature ranking was repeated within the training data of every inner fold. Candidate feature counts were 10, 25, 50, and 100 genes. Candidate elastic-net mixing parameters were alpha=0, 0.5, and 1, representing ridge-dominant, mixed elastic-net, and lasso penalties. Candidate lambda values were 0.01, 0.1, 1, 10, and 100. For each outer development set, an inner leave-one-training-individual-out loop selected the combination of feature count, alpha, and lambda with the lowest pooled inner root mean squared error. The chosen configuration was then refitted using all outer-training donors and used once to predict the outer held-out donor. Elastic-net models were fitted with glmnet.

The ranking statistic within each training partition was derived from donor-adjusted association between expression and absolute PMI using only that partition. Repeating ranking inside the inner loop ensured that the apparent relevance of a gene was not informed by the inner validation donor. The complete procedure therefore nested both feature selection and hyperparameter tuning. Selected configurations were allowed to differ across outer folds, reflecting the model that would be obtained from each available training set rather than imposing information from the full cohort.

Outer-fold predictions from all 54 samples were pooled to calculate root mean squared error (RMSE), mean absolute error (MAE), coefficient of determination (R^2), and Spearman rank correlation. RMSE gave greater weight to large errors, MAE summarised typical absolute deviation in hours, R^2 assessed improvement relative to a constant mean prediction, and Spearman correlation assessed ordinal agreement without substituting for error magnitude or calibration. A negative R^2 indicated that the pooled predictions explained less outcome variation than the corresponding mean-based reference.

A training-mean baseline was calculated separately in every outer fold by assigning the mean absolute PMI of the outer-training donors to each held-out sample. This comparator required no transcriptomic features and represented the performance obtainable from the sampling distribution alone. Differences between elastic-net and baseline RMSE and MAE were reported descriptively. Ninety-five per cent confidence intervals for elastic-net RMSE and MAE were calculated from 2,000 donor-level bootstrap resamples. Each resample selected donors with replacement and retained all serial observations of each selected donor, thereby preserving within-donor dependence. With only seven donor clusters, the intervals were interpreted as descriptive uncertainty rather than precise population bounds.

2.7 Software and reproducibility

All analyses were executed in R 4.5.3. Principal packages were edgeR 4.8.2 for count representation and normalisation, limma 3.66.0 for voom transformation and linear modelling, glmnet 4.1-10 for penalised regression, data.table for data handling, and ggplot2 for visualisation. Functional enrichment used the g:Profiler application programming interface. Random resampling used a fixed seed. The analysis was rerun from the archived GEO series matrix and processed-count files, reproducing cohort counts, eligible-gene totals, sensitivity statistics, prediction metrics, and publication figures. Derived gene-level, pathway-level, sample-level, and fold-level outputs were retained in machine-readable form.

Reproducibility checks were performed at three levels. First, sample accessions, donor labels, and time variables were reconciled before the expression matrix was constructed. Second, all reported totals and estimates were generated directly from saved analytical outputs rather than manually transcribed intermediate calculations. Third, concordance was checked across the abstract, main text, tables, figures, and machine-readable result files. The archived outputs include gene coefficients and adjusted P values, donor-direction counts, complete pathway results, outer-fold predictions, selected fold parameters, and sample-level residuals. This structure permits reconstruction of each reported result and separates the fixed source files from derived analytical products.

3. Results

3.1 Cohort and transcriptome structure

All 54 GEO samples had a unique accession, an identifiable donor, and complete absolute-PMI metadata. Donors contributed nine, nine, nine, nine, seven, eight, and three serial samples, respectively. Absolute PMI ranges differed across individuals: 11.17-35.17 h, 13.58-37.58 h, 13.83-37.83 h, 3.60-27.60 h, 2.35-20.35 h, 3.00-27.00 h, and 18.07-24.07 h. Thus, the combined cohort covered early and later portions of the 2.35-37.83 h range, although no single donor represented every absolute-PMI value. The 0-24 h serial offset described repeat collections from each donor and was not equivalent to time since death.

The count matrix contained 60,204 gene rows before filtering and 12,633 genes after applying the counts-per-million criterion. Library totals ranged from 3.84 to 27.03 million, and detected-gene counts ranged from 12,422 to 17,803 per sample. Principal-component analysis of the 500 most variable expression profiles showed substantial separation related to donor identity, with temporal displacement also visible within several donor trajectories. The cohort structure and donor trajectories are detailed in Figure 1A. This pattern supported donor adjustment in gene-level modelling and complete donor separation in predictive validation. No sample was removed on the basis of the principal-component display.

The sampling structure was uneven by design rather than a balanced repeated-measures experiment. Four donors contributed nine observations across approximately 24 h, two contributed seven or eight observations, and one contributed three observations across 6 h. Early absolute-PMI values were concentrated in Individuals 4-6, whereas Individuals 1-3 contributed more observations above 30 h. Consequently, temporal coverage in the pooled dataset partly overlapped with donor identity. The association model addressed stable donor baselines through fixed effects, while the prediction analysis preserved this real-

world challenge by withholding complete donors rather than artificially balancing or interpolating their trajectories.

3.2 PMI-associated genes

Among the 12,633 expressed genes, 2,065 had a Benjamini-Hochberg adjusted P value below 0.05 for the absolute-PMI coefficient. After adding the prespecified effect-size and directional-consistency requirements, 1,976 genes remained eligible. Of these, 954 increased and 1,022 decreased with advancing absolute PMI. The eligible set therefore represented 15.6% of all expressed genes, with a near-balanced distribution between directions. Donor-centred aggregate signatures showed progressive separation of the increasing and decreasing sets across absolute PMI, while individual trajectories retained visible heterogeneity, as illustrated in Figure 1B.

The leading increasing signals included GADD45G, RHOB, EIF4A3, TBC1D22A-DT, SRPX, GNG12, PNPLA8, and CXCL8. Their effect estimates, false-discovery rates, directions, and donor consistency are detailed in Table 1. Estimated $\log_2$ changes per ten hours ranged from 0.540 for PNPLA8 to 1.970 for SRPX among these representatives. GADD45G, EIF4A3, TBC1D22A-DT, SRPX, and GNG12 had concordant positive slopes in all seven donors, whereas RHOB, PNPLA8, and CXCL8 were concordant in six donors. Representative decreasing genes included TBXAS1, MPEG1, FAM110A, and RHOH, with changes from -0.623 to -0.646 $\log_2$ units per ten hours. MPEG1, FAM110A, and RHOH were directionally concordant in all donors, and TBXAS1 was concordant in six.

The combination of multiplicity control, minimum coefficient magnitude, and donor-level direction produced a narrower gene set than significance testing alone. Eighty-nine of the 2,065 transcripts with adjusted $P < 0.05$ did not meet the complete eligibility definition. The reported coefficients describe relative RNA abundance on the voom $\log_2$ scale after donor adjustment. They do not represent protein fold changes, cell counts, or direct measures of pathway activity.

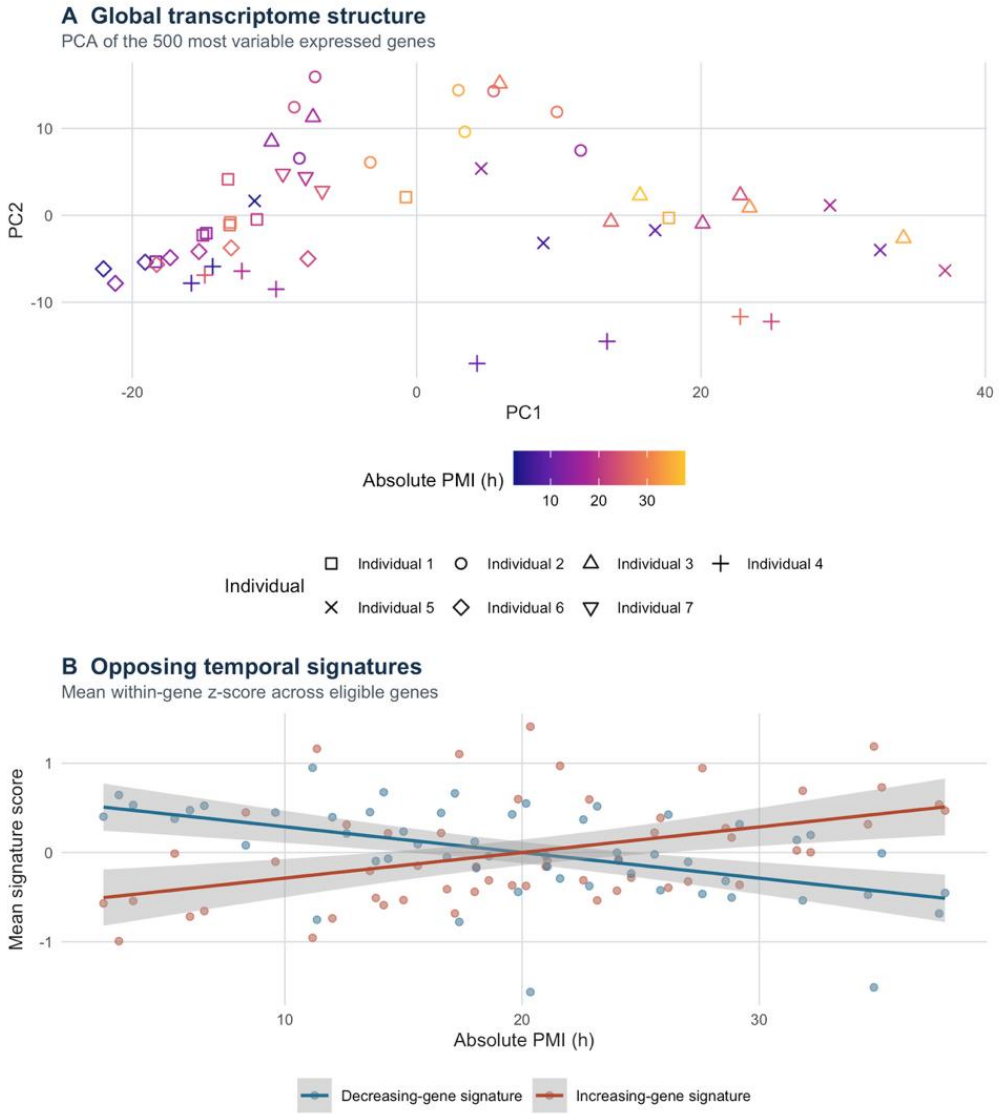

Figure 1. Transcriptome structure and longitudinal signatures. (A) Principal-component analysis of the 500 most variable genes shows strong donor structure across 54 samples; colour represents absolute postmortem interval (PMI, 2.35-37.83 h), not the 0-24 h serial collection offset. (B) Donor-centred aggregate expression of eligible increasing and decreasing genes. Lines connect serial samples within each donor; bold curves show smoothed trends.

Table 1. Leading postmortem interval-associated genes in human blood

Gene	Direction	$\Delta\log_2$/10 h	BH FDR	Consistent donors
GADD45G	Increasing	1.039	8.46e-08	7/7
RHOB	Increasing	1.133	8.46e-08	6/7
EIF4A3	Increasing	0.839	1.28e-07	7/7
TBC1D22A-DT	Increasing	1.055	5.97e-06	7/7
SRPX	Increasing	1.970	9.69e-06	7/7
GNG12	Increasing	1.755	1.10e-05	7/7
PNPLA8	Increasing	0.540	1.30e-05	6/7
CXCL8	Increasing	1.216	2.42e-05	6/7
TBXAS1	Decreasing	-0.646	5.97e-06	6/7
MPEG1	Decreasing	-0.641	7.91e-06	7/7
FAM110A	Decreasing	-0.625	2.36e-05	7/7
RHOH	Decreasing	-0.623	2.36e-05	7/7

Notes: Δlog2/10 h is the donor-adjusted log2 expression change per 10 hours of absolute PMI. BH FDR, Benjamini-Hochberg false-discovery rate; PMI, postmortem interval.

3.3 Sensitivity analysis

The sensitivity dataset excluded six libraries below 50% of the median total and included collection vein as an additional covariate. Across expressed genes, the correlation between primary and sensitivity absolute-PMI coefficients was 0.987. Of the 1,976 eligible genes, 1,645 retained adjusted significance and the same direction, corresponding to 83.2%. The strong coefficient correlation indicated that the overall pattern and ordering of temporal effects changed little under the alternative specification. The smaller retained count reflected both reduced sample information after exclusion and changes in uncertainty after vein adjustment.

3.4 Functional enrichment

The increasing query produced 955 significant terms across the queried resources, whereas the decreasing query produced 652. Representative increasing processes included cytoskeleton in muscle cells, muscle contraction, extracellular-matrix organisation, degradation of the extracellular matrix, response to oxidative stress, mitochondrial ATP synthesis coupled electron transport, and haemostasis, as detailed in Figure 2. These terms incorporated between 13 and 57 query genes in the representative display. The strongest illustrated increasing term, cytoskeleton in muscle cells, had 57 overlapping genes and an adjusted P value of 4.84e-34.

Representative decreasing processes included immune effector process, adaptive immune response, T-cell activation, antigen processing and presentation, and B-cell receptor signalling. The displayed terms incorporated 18-69 query genes. Immune effector process included 69 overlapping genes, adaptive immune response included 60, and T-cell activation included 57. Antigen processing and presentation and B-cell receptor signalling involved smaller but strongly enriched sets. The direction-specific results showed that temporal change was organised across multiple functional systems rather than being confined to a small number of isolated transcripts.

3.5 Cross-donor PMI prediction

Strict nested donor-held-out elastic-net prediction yielded a pooled RMSE of 10.03 h (95% CI 8.12-11.32), MAE of 8.63 h (95% CI 6.33-10.40), R^2 of -0.219, and Spearman rho of 0.380. The complete performance summary is detailed in Table 2, and observed-versus-predicted agreement for all held-out samples is illustrated in Figure 3. The fold-specific training-mean baseline yielded an RMSE of 9.67 h and MAE of 7.85 h. Elastic-net prediction therefore increased RMSE by 0.36 h and MAE by 0.78 h relative to the baseline. The negative R^2 indicated that the cross-donor transcriptomic predictions did not improve on mean-based prediction in explaining pooled absolute-PMI variation.

Prediction error varied across held-out donors. Donor-specific MAE values were 10.11, 8.12, 8.82, 11.38, 11.76, 3.86, and 2.31 h for Individuals 1-7, respectively. The two lowest donor-specific errors occurred in donors whose observed absolute-PMI ranges were comparatively restricted or positioned differently within the cohort. These fold values were descriptive because each donor contributed a different number and range of serial samples. They nevertheless demonstrated that pooled performance combined heterogeneous fold behaviour rather than a uniform error pattern.

The selected hyperparameters also varied by outer fold. Models used 50 or 100 ranked genes; alpha values included 0, 0.5, and 1; and selected lambda values ranged from 0.1 to 10. Inner-fold RMSE values ranged from 6.58 to 8.77 h. Because each configuration was selected only from the available training donors, this variation documented how model composition changed when one donor was removed. The outer predictions retained the full nested structure irrespective of which configuration was selected.

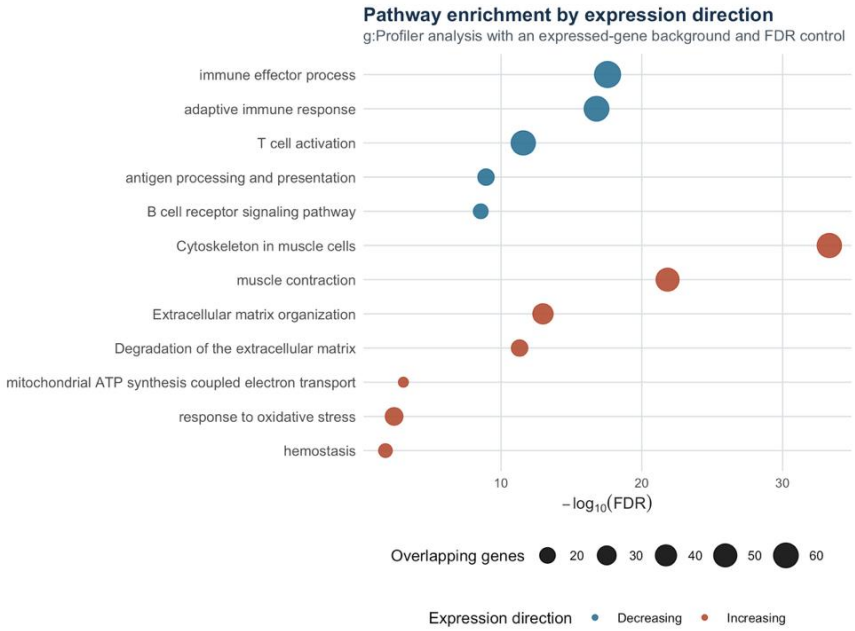

Figure 2. Representative functional enrichment by expression direction. Enrichment used the top 500 eligible genes per direction (495 increasing and 497 decreasing identifiers mapped) against the 12,633 expressed-gene background. FDR, false-discovery rate; GO:BP, Gene Ontology Biological Process; KEGG, Kyoto Encyclopedia of Genes and Genomes.

Table 2. Cross-donor postmortem interval prediction performance

Model	Metric	Estimate	95% CI
Nested elastic net	RMSE, h	10.03	8.12-11.32
Nested elastic net	MAE, h	8.63	6.33-10.40
Nested elastic net	R^2	-0.219	Not estimated
Nested elastic net	Spearman rho	0.380	Not estimated
Training mean	RMSE, h	9.67	Not estimated
Training mean	MAE, h	7.85	Not estimated

Notes: Outer validation held out all serial samples from one donor. The training-mean baseline was recomputed in each outer fold. Confidence intervals use 2,000 donor-level bootstrap resamples and are descriptive because only seven donor clusters were available. CI, confidence interval; MAE, mean absolute error; PMI, postmortem interval; RMSE, root mean squared error.

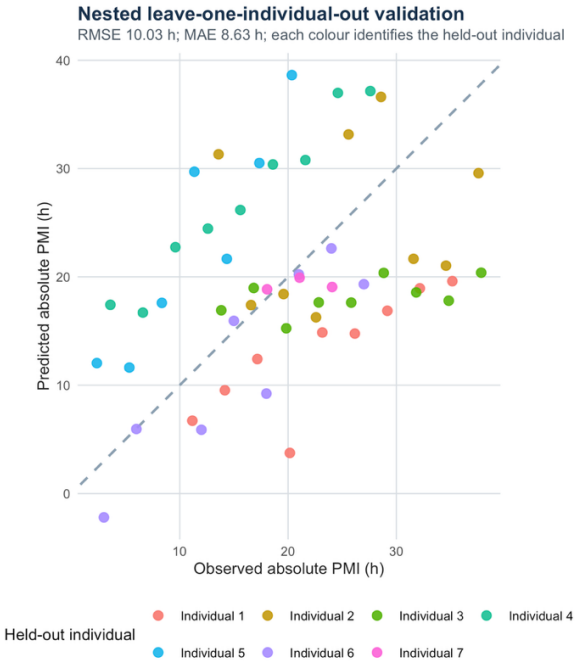

Figure 3. Strict nested leave-one-individual-out prediction of absolute postmortem interval (PMI). All serial samples from each held-out donor were excluded from feature ranking, tuning, and fitting. The dashed line denotes perfect agreement. MAE, mean absolute error; RMSE, root mean squared error.

4. Discussion

This study identified extensive, directionally consistent remodelling of the early human blood thanatotranscriptome but found that these signals did not provide accurate PMI prediction for an unseen donor in the available cohort. Nearly two thousand transcripts met joint criteria for false-discovery rate, effect magnitude, and donor-level direction, and the resulting gene sets were organised into coherent cellular, extracellular-matrix, mitochondrial, oxidative-stress, haemostatic, and immune processes. In contrast, strict donor-held-out elastic-net prediction produced an RMSE of 10.03 h, a negative R^2, and errors exceeding the training-mean baseline. The primary and secondary aims therefore yielded complementary conclusions: the dataset supports reproducible biological change with absolute PMI, while the observed cross-donor signal is not sufficient for case-level time estimation.

The integrated presentation of the results is central to that distinction. Figure 1 shows why donor identity had to be modelled explicitly and why complete donor separation was required for prediction. Table 1 then anchors the pathway interpretation in representative gene-level estimates rather than relying on ontology labels alone. Figure 2 organises those genes into direction-specific biological systems, whereas Table 2 and Figure 3 shift the evidentiary question from association to numerical agreement in held-out donors. Reading these outputs as a sequence prevents the 1,976 eligible transcripts from being interpreted as equivalent to 1,976 validated forensic markers. A candidate marker must retain its temporal direction, provide reproducible assay signal, add predictive information beyond transparent comparators, and remain calibrated when applied to people, settings, and pre-analytical conditions absent from model development. Recent RNA-quality and assay studies reinforce the importance of treating measurement stability and analytical validation as separate requirements from statistical discovery.[8,9,20]

The presence of both increasing and decreasing programmes is consistent with the view that postmortem RNA profiles arise from interacting biological processes rather than uniform transcript loss. Previous multi-tissue studies have documented regulated postmortem expression and tissue-specific responses to death and cold ischaemia.[4-7] The source GSE163207 investigation similarly described coordinated survival and DNA-damage-related activity in postmortem blood.[3] In the present analysis, positive temporal coefficients were distributed across stress-related genes and structural pathways, while negative coefficients were concentrated in immune functions. This directional organisation remained visible after donor centring and was stable when low-library samples were excluded and vein site was added to the model.

Several mechanisms could contribute to the increasing signature. Loss of oxygen and energy homeostasis may activate or preserve transcripts involved in cellular stress before transcriptional capacity ceases. GADD45G is consistent with a cellular stress and damage-response context, while RHOB and cytoskeletal terms may reflect changes in cell shape, membrane organisation, adhesion, or survival signalling. Enrichment of extracellular-matrix organisation and degradation may represent coordinated expression within blood cells, release or persistence of matrix-related transcripts, or shifts in cellular composition. Mitochondrial electron-transport and oxidative-stress terms are biologically compatible with altered redox balance after circulatory arrest. These interpretations remain hypotheses at the transcript level and require targeted experimental confirmation.

The decreasing immune signature was broad, involving adaptive immune response, T-cell activation, antigen processing and presentation, B-cell receptor signalling, and general immune effector processes. A decline in these transcripts could arise through selective degradation, loss of viable immune-cell subsets, redistribution of leukocyte populations, cessation of activation programmes, or differences in stability among transcript classes. The current count matrix cannot separate within-cell transcriptional change from changes in cell mixture. Single-cell or cell-sorted designs could determine whether the observed trajectory reflects coordinated regulation within leukocytes, differential survival of cell populations, or both. Protein-level immune markers would also be needed to establish whether transcript decline corresponds to functional loss.

Pathway enrichment strengthened interpretation by moving from individual genes to coordinated functional themes, but its evidentiary role should remain specific. Over-representation depends on the selected gene threshold, identifier mapping, database coverage, term size, and correlations among genes and ontology categories. The use of an expressed-gene background reduced one source of bias, and separate directional queries avoided combining biologically opposing changes. Even so, enrichment does not measure protein abundance, phosphorylation, enzyme activity, metabolic flux, or causal pathway activation. The results are most useful for prioritising biological systems and constructing candidate panels that can be tested by independent assays.

The sensitivity analysis supports the stability of the gene-level pattern within the observed data. A coefficient correlation of 0.987 indicates that excluding six lower-count libraries and adding vein site produced only modest changes in the overall temporal effect estimates. Retention of adjusted significance and direction for 1,645 eligible genes further indicates that the main result was not dependent on one analytical specification. The reduction from 1,976 eligible genes should be interpreted in the context of fewer samples and an additional covariate, both of which alter standard errors. Sensitivity stability does not remove possible effects of unmeasured pre-analytical variables, but it increases confidence that the leading directional pattern is not explained solely by the specified library-size or collection-site factors.

The contrast between association and prediction is the central methodological finding. The fixed-effect association model compared later and earlier observations within the same donor after accounting for donor-specific baselines. It therefore benefited from the serial design and addressed whether expression changed systematically with absolute PMI. A new-case prediction model cannot condition on the unknown donor's prior samples. It must distinguish temporal position from inter-individual variation using only patterns learned from other people. Strong within-donor slopes can coexist with higher-error cross-donor prediction whenever baseline differences are large relative to the shared temporal component or when temporal trajectories vary in magnitude and shape between individuals.

Validation strategy determines which of these questions is answered. Randomly distributing correlated samples from the same donor across training and test sets permits

donor-specific molecular characteristics to appear on both sides of the evaluation. A model can then benefit from proximity to that donor's training observations even if the learned relation does not transfer to another person. The nested leave-one-individual-out procedure used here excluded the held-out donor from ranking, hyperparameter selection, and fitting. The resulting estimate is consequently aligned with the intended forensic question of performance in a person not previously observed by the model. This design is demanding, but it makes the prediction target explicit and clinically interpretable.

The source study reported an RMSE of approximately 4.75-4.88 h under its analytical validation design.[3] That estimate and the present RMSE of 10.03 h need not be viewed as contradictory because they quantify different generalisation targets. The source estimate describes performance under the source partitioning and model-development procedure, whereas the present value describes transfer to a completely excluded donor with feature selection and tuning nested within training donors. The larger error therefore provides additional information about donor transportability. It does not negate the biological findings of the source study or the value of GSE163207 as a longitudinal discovery resource.

The baseline comparison is also informative. The training-mean predictor used no RNA information and achieved lower RMSE and MAE than the elastic-net model. This result indicates that the transcriptomic features, as combined in the present cohort, did not improve absolute-PMI estimation beyond the centre of the training distribution. Spearman rho of 0.380 suggests partial ordinal information, but correlation alone does not quantify agreement or absolute error. The negative R^2 shows that this ordinal tendency did not translate into an overall improvement in squared prediction error. For forensic use, a model must be evaluated on error magnitude, calibration, and performance relative to transparent comparators, not only on correlation or statistical association.

Variation in fold-specific error and selected hyperparameters further illustrates the effect of donor composition. Removing one individual changed which genes and penalties were preferred by inner validation, with feature counts of 50 or 100 and alpha values spanning ridge, elastic-net, and lasso solutions. This is expected when the development set contains only six donors per outer fold and each donor contributes a distinct temporal range and molecular background. The observation does not identify a single preferred penalty; instead, it indicates that model specification is responsive to the limited donor sample. Larger training cohorts would allow more stable evaluation of feature recurrence, shrinkage strength, nonlinear time effects, and calibration.

From a biomarker-development perspective, the findings favour pathway-informed candidate selection followed by independent measurement rather than direct deployment of the high-dimensional predictor. A parsimonious panel could include representatives of stress and damage response, immune decline, mitochondrial function, and cytoskeletal or extracellular-matrix change, together with reference transcripts shown to be stable after death. Candidate genes should be assessed for assay efficiency, abundance, degradation kinetics, and sensitivity to blood-cell composition. RT-qPCR or digital PCR could provide a practical platform for targeted validation after sequencing-based discovery.[20] Current reviews similarly emphasise assay standardisation, stable normalisers, environmental characterisation, and external validation for RNA-based PMI methods.[1,2]

Future prediction studies should prospectively define the intended use before model construction. Relevant choices include whether the target is continuous absolute PMI or a clinically meaningful interval, the maximum acceptable error, the postmortem window, the anatomical sampling site, and the conditions under which the model would be applied. Training and validation cohorts should record temperature, storage, time to preservation, RNA integrity, cause and manner of death, resuscitation, infection, medication, age, sex, and other variables that may influence blood-cell transcription. Temperature-dependent RNA degradation has been demonstrated in postmortem tissue and should be incorporated into study design rather than treated as an unmeasured background condition.[8]

A multicentre design would provide the clearest next step for transportability. Discovery and internal tuning could occur in several centres while an entire institution, geographic setting, or collection period is reserved for external validation. Repeated samples should remain grouped by donor in every split. Model evaluation should report MAE, RMSE, calibration intercept and slope, error across prespecified PMI ranges, and uncertainty at the donor level. Transparent baselines should be included, and a molecular model should demonstrate incremental value over readily available contextual variables. If multimodal models are developed, transcriptomic information can be combined with temperature, biochemical markers, proteins, metabolites, microRNAs, or conventional postmortem findings, provided each component is collected prospectively and validated without leakage.[21-31] Emerging microRNA research offers one possible complementary molecular layer.[11,15,16]

The study has several strengths. It uses a rare serial human dataset, distinguishes absolute PMI from sampling offset, retains all available observations in the primary analysis, and makes the donor the unit of predictive generalisation. Gene selection combines multiplicity control, effect magnitude, and directional evidence. Enrichment uses the expressed transcriptome as background and reports the actual capped and mapped query sizes. The sensitivity model addresses two documented analytical factors, while prediction nests both ranking and tuning. Finally, the interpretation separates evidence for biological remodelling from evidence for individual time estimation, allowing positive molecular findings and non-improving predictive performance to be reported within one coherent framework.

Interpretation is bounded by the available cohort. Seven individuals provide detailed serial observations but limited coverage of population heterogeneity, and donor ages were 56-89 years. The study was conducted in one source setting, with recorded ancestry and clinical context that may not represent other populations. Cause-of-death information and several premortem variables were not available in the processed analytical metadata. Source vein varied, and the processed-count analysis did not include read-level alignment metrics, RNA integrity numbers, or a complete technical-batch structure. These conditions affect the range of settings to which the estimates can be transported, particularly field cases with different temperatures, delays, tissues, or preservation procedures.

The donor-level bootstrap intervals also reflect only seven independent clusters. They appropriately preserve serial

dependence, but their numerical width should not be interpreted as definitive population precision. The gene-association findings are observational, and pathway results do not establish causality. Processed counts prevented assessment of alternative transcript isoforms, mapping artefacts, fragment-level degradation, and sequence quality. No independent external cohort was available to test the identified genes, pathway signatures, or elastic-net model. These considerations define the next validation requirements while leaving the observed within-cohort temporal pattern and the reported cross-donor performance directly interpretable.

Overall, the results support a staged translational interpretation. At the discovery stage, the human blood thanatotranscriptome contains broad and reproducible temporal organisation. At the candidate-panel stage, the directionally consistent genes and pathways provide rational targets for assay development. At the predictive-validation stage, the present model does not add accuracy beyond a mean-based reference for an unseen donor. Maintaining these stages prevents biological association from being overextended into an individual forensic estimate and directs future effort toward donor diversity, pre-analytical control, parsimonious assays, multimodal integration, and genuinely external validation.

5. Conclusion

Human blood undergoes extensive and directionally consistent transcriptomic remodelling across an absolute PMI of 2.35-37.83 h. Increasing signals involved cytoskeletal, extracellular-matrix, oxidative-stress, mitochondrial, and haemostatic processes, whereas decreasing signals involved adaptive immune function and antigen presentation. These associations remained stable in sensitivity analysis. However, strictly nested prediction in completely held-out donors produced an RMSE of 10.03 h, MAE of 8.63 h, and negative R^2 and did not improve on the training-mean baseline. The findings support GSE163207 as a resource for biological discovery and candidate-panel development, while indicating that individual PMI estimation requires larger, diverse, prospectively characterised cohorts and external donor-level validation.

Declarations

Use of generative artificial intelligence. No generative artificial intelligence tool was used in the conception, design, analysis, drafting, revision or preparation of this manuscript. The authors accept full responsibility for the content of the article.

Author contributions. Both authors (RH and KA) contributed to the study design, analysis, and drafting, and both reviewed and approved the final manuscript.

Funding. This research received no specific grant from any funding agency in the public, commercial, or not-for-profit sectors.

Conflict of interest. The authors declare no competing interests.

Ethical approval. The source study reported approval by the Ethical Commission of the University Hospitals Leuven (S58486) and informed consent before donation. Ethical approval for this secondary reanalysis was granted by the CMHC Ethics Committee Indonesia (No. 009/CMHC/Ethics/08/2026).

Consent for publication. Not applicable; no identifiable individual information is reported.

Data availability. The source counts and metadata are publicly available from NCBI GEO under accession GSE163207. Reproducible analysis code and derived tables are retained in the case archive and can be supplied to the journal.

Acknowledgements. The authors acknowledge the original investigators and donors who made GSE163207 publicly available.

References

1. Mróz M, Miodońska M, Cieśla J, et al. As precisely as possible! Molecular methods of postmortem interval prediction-current prospects and limitations. J Forensic Leg Med. 2025;115:102946. doi: 10.1016/j.jflm.2025.102946.
2. Cianci V, Mondello C, Sapienza D, et al. Potential role of mRNA in estimating postmortem interval: a systematic review. Int J Mol Sci. 2024;25(15):8185. doi: 10.3390/ijms25158185.
3. Antiga LG, Sibbens L, Abakkouy Y, et al. Cell survival and DNA damage repair are promoted in the human blood thanatotranscriptome shortly after death. Sci Rep. 2021;11(1):16585. doi: 10.1038/s41598-021-96095-z.
4. Zepeta Flores N, Garduño Zarazúa LM, Piñón Zarate G, et al. Transcriptomic analysis at 48 h postmortem: a proof of concept for the identification of biomarkers to estimate time since death. Mol Biol Rep. 2025;52(1):1050. doi: 10.1007/s11033-025-11151-5.
5. Choi S, Jung M, Jeong M, et al. Postmortem changes in mRNA expression and tissue morphology in brain and femoral muscle tissues of rat. Int J Mol Sci. 2025;26(15):7059. doi: 10.3390/ijms26157059.
6. Sato K, Sugasawa T, Wan J, et al. Temporal and spatial RNA expression dynamics in postmortem skin support PMI estimation and reveal spatial signatures of antemortem injury. Int J Legal Med. 2026. doi: 10.1007/s00414-026-03896-w.
7. Javan GT, Bethea J, Cecchetto G, et al. A transcriptome-wise atlas of human prostate as a function of postmortem interval time. Sci Rep. 2025;16(1):299. doi: 10.1038/s41598-025-29561-7.
8. Jacobsen SB, Tfelt-Hansen J, Smerup MH, et al. RNA degradation patterns in cardiac tissues kept at different time intervals and temperatures before RNA sequencing. PLoS One. 2025;20(5):e0323786. doi: 10.1371/journal.pone.0323786.
9. Tian J, Lam TG, Ross SK, et al. An analysis of RNA quality metrics in human brain tissue. J Neuropathol Exp Neurol. 2025;84(3):236-243. doi: 10.1093/jnen/nlae132.
10. Olney KC, Gibson KA, Cadiz MP, et al. Postmortem interval leads to loss of disease-specific signatures in brain tissue. eNeuro. 2025; 12(3): ENEURO.0505-24.2025. doi: 10.1523/ENEURO.0505-24.2025.
11. Lee H, Lee EJ, Park K, et al. MicroRNA transcriptome analysis for post-mortem interval estimation. Forensic Sci Int. 2025;370:112473. doi: 10.1016/j.forsciint.2025.112473.
12. Gao H, Yang S, Gao J, et al. An experimental study to estimate the early postmortem interval based on the degradation of lncRNAs in rat brain tissue. Sci Rep. 2024;14(1):19586. doi: 10.1038/s41598-024-70678-y.
13. Song B, Fu J, Cheng J, et al. Circular RNA circFat3 as a biomarker for construction of postmortem interval estimation models in mouse brain tissues at multiple temperatures. Sci Rep. 2025;15(1):21577. doi: 10.1038/s41598-025-07998-0.
14. Song B, Fu J, Qian J, et al. Development of mathematical models using circRNA combinations (circTulp4, circSlc8a1, and circStrn3) in mouse brain tissue for postmortem interval estimation. Int J Mol Sci. 2025;26(10):4495. doi: 10.3390/ijms26104495.
15. Lee EH, Jeong M, Park K, et al. Detection of miR-133a-5p using a molecular beacon probe for investigating postmortem intervals. Noncoding RNA. 2024;10(6):58. doi: 10.3390/ncrna10060058.
16. Wang Y, Li B, Wang Y, et al. Endogenous and exogenous small RNA signatures as novel tools for postmortem interval determination. Biomolecules. 2026;16(3):474. doi: 10.3390/biom16030474.
17. Yin M, Gao H, Chen J, et al. Experimental study of mRNA from human dental pulp tissue for late postmortem interval estimation. Sci Rep. 2026;16(1):14398. doi: 10.1038/s41598-026-46591-x.

18. Devi V, Gupta T, Kaur UJ, et al. Time since death estimation via mRNA expression of GAPDH and ACTB in human skeletal muscle. Clin Anat. 2026;39(3):282-292. doi: 10.1002/ca.70026.

19. Buyko EE, Perina EA, Sobakin DS, et al. Dynamics of postmortem gene expression in normal and neoplastic murine liver. Life (Basel). 2026;16(4):683. doi: 10.3390/life16040683.

20. Gao N, Huo Y, Yu D, et al. Evaluation of reverse transcription yield of RNA standards and forensic samples based on droplet digital PCR. Biochem Biophys Res Commun. 2024;711:149909. doi: 10.1016/j.bbrc.2024.149909.

21. M Løber IM, Hedemann MS, Villesen P, et al. Untangling the postmortem metabolome: a machine learning approach for accurate PMI estimation. Anal Chem. 2025;97(30):16123-16132. doi: 10.1021/acs.analchem.4c05796.

22. Fu Y, Wu Z, Wei Y, et al. Untargeted and targeted metabolomics analysis of CO poisoning and mechanical asphyxia postmortem interval biomarkers in rat and human plasma by GC-MS. J Pharm Biomed Anal. 2024;251:116443. doi: 10.1016/j.jpba.2024.116443.

23. Fan W, Dai X, Ye Y, et al. Estimation of postmortem interval under different ambient temperatures based on multi-organ metabolomics and machine learning algorithm. Int J Legal Med. 2025;139(5):2561-2575. doi: 10.1007/s00414-025-03523-0.

24. Lu XJ, Li J, Wei X, et al. A novel method for determining postmortem interval based on the metabolomics of multiple organs combined with ensemble learning techniques. Int J Legal Med. 2023;137(1):237-249. doi: 10.1007/s00414-022-02844-8.

25. Mazzatenta A, Pietrangelo T, Demontis R, et al. Volabolomic fingerprinting for post-mortem interval estimation: a novel physiological approach. Biomolecules. 2024;14(3):286. doi: 10.3390/biom14030286.

26. Garcés-Parra C, Saldivia P, Hernández M, et al. Enhancing late postmortem interval prediction: a pilot study integrating proteomics and machine learning to distinguish human bone remains over 15 years. Biol Res. 2024;57(1):75. doi: 10.1186/s40659-024-00552-8.

27. Wang X, Le C, Jin X, et al. Estimating postmortem interval based on oral microbial community succession in rat cadavers. Heliyon. 2024;10(11):e31897. doi: 10.1016/j.heliyon.2024.e31897.

28. Iancu L, Bonicelli A, Procopio N, et al. Decomposition in an extreme cold environment and associated microbiome-prediction model implications for postmortem interval estimation. Front Microbiol. 2024;15:1392716. doi: 10.3389/fmicb.2024.1392716.

29. Rose S, Johnson H, Cartozzo C, et al. Testing the efficacy of surface swab sampling to determine postmortem submersion interval using microbiome colonization of skeletal remains. J Forensic Sci. 2025;70(4):1261-1273. doi: 10.1111/1556-4029.70039.

30. Xia Y, Chen S, Deng Z, et al. Soil microbial succession for forensic estimation of postmortem interval and decomposition site identification. Int J Legal Med. 2026. doi: 10.1007/s00414-026-03807-z.

31. Nieciecki V, Seitz VA, Burcham ZM, et al. Insects shape the cadaver decomposition microbiome and postmortem interval estimation accuracy. mSystems. 2026;11(5):e00681-25. doi: 10.1128/msystems.00681-25.